ELSEVIER

Journal of Chromatography A, 897 (2000) 81–97

JOURNAL OF CHROMATOGRAPHY A

www.elsevier.com/locate/chroma

Protein adsorption on novel acrylamido-based polymeric ion exchangers
II. Adsorption rates and column behavior

Alan K. Hunter, Giorgio Carta*

Department of Chemical Engineering, University of Virginia, Thornton Hall, Charlottesville, VA 22903-2442, USA

Received 26 January 2000; received in revised form 30 May 2000; accepted 17 July 2000

Abstract

Uptake kinetics and breakthrough behavior were determined for bovine serum albumin (BSA) and α-chymotrypsinogen (αCHY) in new polymeric ion-exchange media based on acrylamido monomers. Two anion exchangers and a cation exchanger were investigated. As shown in Part I of this work, the two anion exchangers have different morphologies. The first one, BRX-Q, comprises a low-density gel with a matrix of denser polymeric aggregates. While this material has a very low size-exclusion limit for neutral probes, it exhibits an extremely high binding capacity for BSA. The second anion exchanger, BRX-QP, comprises large open pores but has a very low binding capacity. The cation exchanger, BRX-S, also comprises large open pores but exhibits an intermediate capacity; likely as a result of the presence of smaller pores. Dynamic protein uptake experiments showed that the highest mass transfer rates are obtained with BRX-Q. The apparent diffusivity is also highest for this material and increases substantially as the protein concentration is reduced. For these particles, the external film resistance is dominant at very low protein concentrations. Much lower rates and apparent diffusivities are obtained for BRX-QP. Finally intermediate rates and apparent diffusivities are found with BRX-S. The concentration dependence of the apparent pore diffusivity is much less pronounced in this case. The apparently paradoxical result that mass transfer rates are highest for the material with the smallest neutral-probe size-exclusion limit can be explained in terms of a general conceptual model where parallel pore and adsorbed-phase diffusion paths exist in these particles. In the first case, adsorbed phase diffusion in gel pores is dominant, while in the second transport is dominated by diffusion in a macroporous network. In the third case, both contributions are important. The conceptual model provides an accurate prediction of the breakthrough behavior of columns packed with these media using independently determined rate parameters. Dynamic binding capacities of 80–140 mg/ml were observed for BSA on BRX-Q in ca. 1.5 cm columns operated at 300–900 cm/h in agreement with theoretical predictions.

Keywords: Diffusion; Ion exchangers; Polymeric gels; Adsorption; Stationary phases, LC; Proteins

1. Introduction

In Part I of this work [1], we have characterized morphological and adsorptive properties of new

*Corresponding author. Tel.: +1-804-9246-281; fax: +1-804-9822-658.

E-mail address: gc@virginia.edu (G. Carta).

0021-9673/00/$ – see front matter
PII: S0021-9673(00)00865-7

stationary phases for protein ion-exchange chromatography based on hydrophilic acrylamido monomers. By examining these materials, we inferred that a variety of structures can be obtained. One of the observed structures comprises a lower-density polymer–gel phase, which provides adsorption sites, surrounded by denser polymer aggregates, which provide mechanical strength. Another structure comprises dense aggregates defining a network of open macropores. Finally, a structure comprising both macropores and smaller pores was inferred. With regard to adsorptive properties, the capacity was very high for particles containing a low-density polymer–gel phase. Such particles nearly completely excluded neutral macromolecules, such as dextrans. However, they adsorbed bovine serum albumin (BSA) very effectively yielding a maximum capacity of 280–290 mg/ml. Conversely, particles containing predominately macropores, while having a very high size-exclusion threshold exhibited a low protein adsorption capacity.

In addition to adsorptive capacity, a knowledge of mass transfer rates is also critically important for assessing the performance of ion-exchange media. This is particularly true for preparative and process-scale applications at high velocities. A number of studies have been devoted to protein mass transfer in chromatography media (e.g., Refs. [2–8]). The ability to make a priori predictions of intraparticle transport rates, however, remains elusive. Chang and Lenhoff [9], for example, recently noted that while mean pore size significantly influences uptake dynamics in ion exchangers, other factors, such as pore connectivity and adsorption affinity, are also important. In general, for macroporous structures, these factors can be accounted for explicitly with network models [10]. Significant uncertainties, however, remain for materials containing small pores, where solute–adsorbent interactions can have an enormous influence. This is especially true for stationary phases containing a gel-porosity that cannot be thought of as a rigid pore network. The concept of ''surface diffusion'' or diffusion in an ''adsorbed phase'' has also been advanced as a conceptual model to describe protein uptake dynamics in polymer gels and rigid pore media [5,7,11,12]. Some direct experimental evidence of such a mechanism has been obtained recently for protein diffusion in charged polyacrylamide gels [13]. However, we are still far from being able to predict the magnitude of these effects for commercial media.

Thus, in this work we have conducted experimental determinations of protein uptake rates using the stationary phases characterized in Part I [1]. A comparison of transport rates for particles having different structures and adsorption equilibrium characteristics is of special interest. Since the morphology is known, these media provide an opportunity to gain some insight of the effect of structure on intraparticle protein transport and on the ability of various rate models to describe batch and column adsorption behavior.

2. Materials and methods

The stationary phases used in this work are the same as those considered in Part I [1] and were obtained from Bio-Rad Labs. (Hercules, CA, USA). They comprise the two polymeric anion exchangers BRX-Q and BRX-QP, and the polymeric cation exchanger BRX-S. All three are based on water-soluble, hydrophilic acrylamido and vinylic monomers. However, they have different morphology as evident from transmission electron microscopy (TEM) and size-exclusion chromatography (SEC) studies. In particular, BRX-Q has a very low size-exclusion limit for neutral probe molecules (~4 nm probe viscosity radius), while BRX-QP has an open macropore structure with a size-exclusion limit much greater than 20 nm. BRX-S also contains a distribution of macropores with some pores on the order of 1 μm, although it also contains smaller pores or a gel-porosity. The adsorption capacity is extremely high (280–290 mg BSA/ml) for BRX-Q and low (~60 mg BSA/ml) for BRX-QP. These differences were attributed to different binding mechanisms: adsorption in a charged-polymer gel in the case of BRX-Q and adsorption on the surface of macropores in the case of BRX-QP. BRX-S had an adsorption capacity of 120–130 mg α-chymotrypsinogen (αCHY)/ml. All three media comprise spherical particles with mean diameters of 89, 98 and 63 μm for BRX-Q, BRX-QP and BRX-S, respectively. Other structural parameters and adsorption isotherms at different salt concentrations are given in Part I of

this work [1]. It should be noted that while a direct comparison of adsorption capacity for media with cationic and anionic chemistries is in general not meaningful, a useful comparison of transport properties and, in particular, of diffusion rates and mechanisms can be made.

The protein used were as in Part I of this work. BSA (Fraction V powder, catalog No. A-6918) and αCHY (Type II, catalog No. C-4879) were obtained from Sigma (St. Louis, MO, USA) and used without further purification. The purity stated by the manufacturer was >98% for both proteins. Molecular masses and isoelectric points are M_r~65 000 and pI~5 for BSA and M_r~26 500 and pI~9.5 for αCHY [14]. Other chemicals were obtained from Sigma and from Fisher Scientific (Pittsburgh, PA, USA). Experiments were done at pH 8.5 in a 50 mM Tris–HCl buffer for the anion exchangers and at pH 6.5 in a 10 mM Na_2HPO_4 buffer for the cation exchanger.

Protein uptake rates were measured in a stirred batch apparatus as well as in a shallow-bed apparatus, which are shown schematically in Fig. 1. Weaver Jr. and Carta [8] and Lewus et al. [15] give technical details of the equipment used. In the stirred-batch apparatus, a sample of clean stationary phase is added to a stirred protein solution whose UV absorbance is followed continuously by circulating a stream through a spectrophotometric detector. The amount of protein adsorbed is obtained by material balance from the change in protein solution concentration. In our experiments we used 0.2–0.5 ml of media with 100 ml of solution stirred at 300 rpm.

In the shallow-bed apparatus, the stationary phase is contained in a very small packed bed. The protein solution is fed at a high flow-rate for a desired period of time. Excess protein is then quickly removed from the extraparticle interstices by feeding a buffer solution to the column. This is followed by a salt solution (500 mM NaCl), which causes elution of the adsorbed protein. The amount adsorbed during the time of exposure to the protein solution is obtained by integrating the salt elution peak monitored with a chromatographic detector. In this case, adsorption occurs with a constant external protein concentration and for hydrodynamics conditions similar to a column operation. We utilized a Pharmacia Model HR 5/5 glass column (Pharmacia, Piscataway, NJ, USA), 5 cm×0.5 cm with two adjustable adapters. The media volume in the shallow-bed assembly was around 5–10 μl. This volume was inserted with a micropipetter and sandwiched between two 0.75 cm layers of PTFE beads, 80–100 μm in diameter, which match that of the particles. Flow-rates in the range 4–8 ml/min were used giving mobile phase velocities in the range 1000–2500 cm/h. A modified ProSys Chromatography workstation, obtained from BioSepra (Marlborough, MA, USA), was used to supply protein, buffer and salt elution solutions [15].

Breakthrough experiments were also conducted in

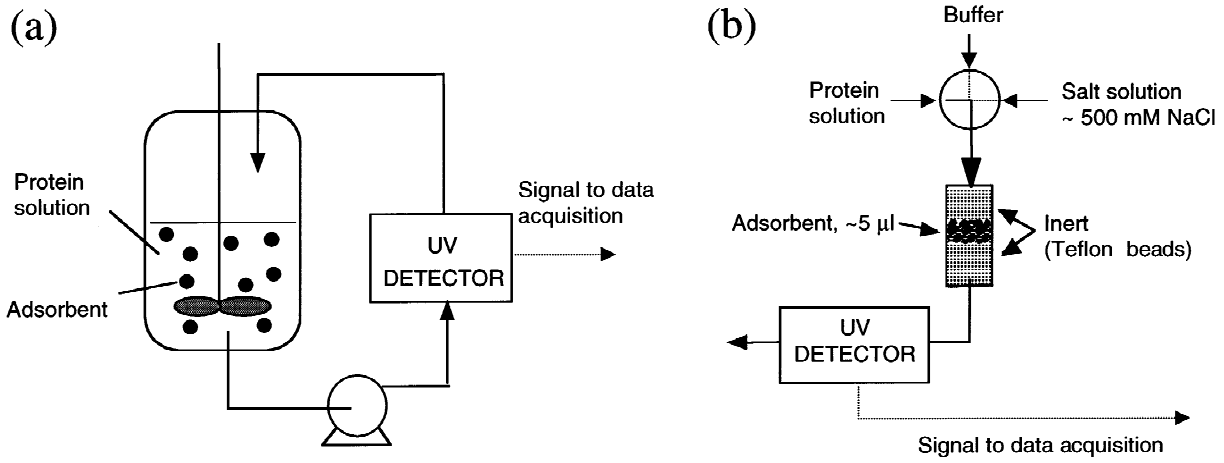

Fig. 1. Schematic of stirred-batch (a) and shallow-bed apparatus (b).

0.5 cm I.D. glass columns packed to a height of 1.5–5.0 cm (Pharmacia, Models HR 5/5 and HR 5/10). The columns were slurry-packed and allowed to equilibrate at a flow-rate of 3 ml/min. An adapter was then lowered to minimize dead volume. Breakthrough curves were monitored through the ProSys UV detection module at 280 nm. The UV absorbance was a linear function of protein concentration for these conditions. The bulk packing density was determined by removing the packing and measuring the dry weight.

3. Theoretical development

3.1. Model

Multiple resistances potentially affect mass transfer between mobile and stationary phases [16,17]. Moreover, adsorption rates are affected by particle size and by the adsorption isotherm. Thus, in order to obtain a meaningful comparison of intrinsic transport properties, it is desirable to analyze experimental data in terms of suitable models. A fairly general description of mass transfer rates in batch adsorption is given by the following equations and boundary conditions [17]:

$$\frac{\partial q}{\partial t} = \frac{1}{r^2} \cdot \frac{\partial}{\partial r} \cdot \left[r^2 \left(D_e \cdot \frac{\partial c}{\partial r} + D_s \cdot \frac{\partial q}{\partial r} \right) \right] \quad (1)$$

$$t = 0: c = 0, q = 0 \quad (1a)$$

$$r = 0: \frac{\partial c}{\partial r} = 0 \quad (1b)$$

$$r = r_p: D_e \cdot \frac{\partial c}{\partial r} + D_s \cdot \frac{\partial q}{\partial r} = k_f \cdot (C - c) \quad (1c)$$

$$\frac{dC}{dt} = -\frac{V_M}{V} \cdot \frac{d\bar{q}}{dt} = -\frac{3k_f}{r_p} \cdot \left(C - c|_{r=r_p} \right) \quad (2)$$

$$t = 0: C = C_0 \quad (2a)$$

The same equations apply to column operation, except that the following differential balance replaces the batch balance in Eq. (2):

$$\epsilon_b \cdot \frac{\partial C}{\partial t} + (1 - \epsilon_b) \cdot \frac{\partial \bar{q}}{\partial t} + u \cdot \frac{\partial C}{\partial z} = \epsilon_b D_L \cdot \frac{\partial^2 C}{\partial z^2} \quad (3)$$

$$t = 0: C = 0 \quad (3a)$$

$$z = 0: uC_F = uC - \epsilon_b D_L \cdot \frac{\partial C}{\partial z} \quad (3b)$$

$$z = L: \frac{\partial C}{\partial z} = 0 \quad (3c)$$

Eq. (1) is based on a conceptual model assuming parallel pore and surface diffusion mechanisms in the particle neglecting accumulation in the intraparticle macropores. The model reduces to the so-called ''pore-diffusion model'' when $D_s = 0$ and to the ''homogeneous'' or ''solid diffusion model'' when $D_e = 0$ [17]. In principle, each of the three rate parameters k_f, D_e, and D_s, is concentration dependent [7]. In practice, however, k_f is primarily dependent on hydrodynamics and is constant with adsorbate concentration unless the solution viscosity varies considerably. Furthermore, for diffusion in reasonably large pores, D_e, which in this model is expected to be lower than the protein free solution diffusivity, is essentially independent of concentration so long as blocking by adsorbed molecules does not occur. If such effects are present, D_e can be predicted from hindered diffusion models and pore-connectivity considerations [10,18]. Finally, while it is difficult to make a priori predictions of D_s, order-of-magnitude estimates can be made. Miyabe and Guiochon [7] reported values of D_s for BSA in a porous ion exchanger in the range 10^{-10}–10^{-9} cm^2/s, but these values were found to increase with the adsorbed protein concentration. Higher values for $D_s = 1 \cdot 10^{-8}$–$5 \cdot 10^{-8}$ cm^2/s, were reported for adsorption of BSA, ovalbumin and lactalbumin in polyacrylamide gel/silica composite ion exchangers [19] and for diffusion of cytochrome *c* in charged polyacrylamide gels immobilized in quartz capillaries [13]. It should be noted that while the D_s values are typically much smaller than protein solution diffusivities [20], surface diffusion can still be significant or even dominant when the adsorbed-protein concentration is much larger then the fluid-phase concentration or when D_e is very small [8].

To complete the description of adsorption rates, the relationship between adsorbed and pore-fluid protein concentration must be defined. Most authors assume local equilibrium for protein adsorption on ion exchangers, and Miyabe and Guiochon [7] have

corroborated this assumption in their detailed study. In this case, the q derivatives in Eqs. (1) and (2) can be expressed through the adsorption isotherm as derivatives of c.

A final consideration regards the dependence of intraparticle transport parameters on the mobile phase velocity. Firstly, a possibility to be considered is that increasing mobile phase velocity causes compression or a structural collapse of the media leading to reduced mass transfer rates. Secondly, we must consider the possibility of intraparticle convection enhancing mass transfer at elevated flow-rates of the mobile phase [21–24]. For spherical particles with a linear isotherm, this effect can be expressed using a convection-augmented diffusivity, $D_{e,conv}$, in lieu of D_e in Eq. (1). The latter is given by [22]:

$$\frac{D_{e,conv}}{D_e} = \frac{Pe_{intra}}{3} \cdot \left(\frac{1}{\tanh Pe_{intra}} - \frac{1}{Pe_{intra}} \right)^{-1} \tag{4}$$

where $Pe_{intra} = Fur_p / 3D_e$ is an intraparticle Peclet number, u is the mobile phase superficial velocity, and F is the ratio of intraparticle and bed mobile phase velocities. This expression can also be used to describe the effects on breakthrough curves with a favorable isotherm [25]. In either case, as shown by Carta and Rodrigues [26], a significant enhancement of mass transfer rates does not occur until $Pe_{intra} \sim 10$ and only at $Pe_{intra} \sim 30$ are convection and diffusion about equal in magnitude. At higher values of Pe_{intra}, Eq. (4) approaches the asymptote:

$$D_{e,conv} = \frac{1}{9} F u r_p \tag{5}$$

in approximate agreement with the result of Frey et al. [24]. For these conditions, intraparticle pore transport is directly proportional to the mobile phase flow-rate. Finally, the parameter F can be estimated from the particle and bed porosities as [22,24]:

$$F = 9 \cdot \left(\frac{\epsilon_p}{\epsilon_b} \right)^3 \cdot \left(\frac{1 - \epsilon_b}{1 - \epsilon_p} \right)^2 \cdot \left(\frac{r_{pore}}{r_p} \right)^2 \tag{6}$$

where r_{pore} is the mean pore radius.

3.2. Asymptotic solutions

In general, the solution of Eqs. (1)–(3) has to be obtained numerically because of the non-linearity of the isotherm. Asymptotic solutions exist, however, for limiting cases and facilitate the analysis of experimental data. For negligible surface diffusion and a rectangular adsorption isotherm the following solutions are found [17]:

For batch adsorption:

$$\frac{D_e C_0}{r_p^2 q_m} \cdot t = \left(1 - \frac{1}{Bi} \right) \cdot I_2 - I_1 \tag{7}$$

where:

$$I_1 = \frac{1}{6\lambda\Lambda} \cdot \ln \left[\frac{\lambda^3 + \eta^3}{\lambda^3 + 1} \cdot \left(\frac{\lambda + 1}{\lambda + \eta} \right)^3 \right] + \frac{1}{\lambda\Lambda\sqrt{3}} \cdot \left[\tan^{-1} \left(\frac{2\eta - \lambda}{\lambda\sqrt{3}} \right) - \tan^{-1} \left(\frac{2 - \lambda}{\lambda\sqrt{3}} \right) \right] \tag{7a}$$

$$I_2 = \frac{1}{3\Lambda} \cdot \ln \left(\frac{\lambda^3 + \eta^3}{\lambda^3 + 1} \right) \tag{7b}$$

$$\eta = \left(1 - \frac{\bar{q}}{q_m} \right)^{1/3} \tag{7c}$$

$$\Lambda = \frac{V_M q_m}{V C_0} \tag{7d}$$

$$\lambda = \left(\frac{1}{\Lambda} - 1 \right)^{1/3} \tag{7e}$$

$$Bi = \frac{k_f r_p}{D_e} \tag{7f}$$

For shallow-bed adsorption:

$$\frac{D_e C_0}{r_p^2 q_m} = \frac{1}{2} - \frac{1}{3} \cdot \left(1 - \frac{1}{Bi} \right) \cdot \frac{\bar{q}}{q_m} - \frac{1}{2} \cdot \left(1 - \frac{\bar{q}}{q_m} \right)^{2/3} \tag{8}$$

In these equations, q_m is the adsorption capacity. Weber and Chakravorti [27] give the corresponding analytical expressions for the breakthrough curve neglecting axial dispersion. Note that Bi is typically quite large. Thus, in the absence of surface diffusion the external resistance is usually significant only for very short times or in the very early portion of the breakthrough curve.

When surface diffusion controls and the isotherm is non-linear, analytical solutions are only available for the case of negligible external resistance [17]. An approximate solution of the breakthrough curve

based on a linear-driving-force approximation also exists for the case of a rectangular isotherm [28]. Otherwise, a numerical solution is required. Finally, the case of parallel pore and surface diffusion generally requires a numerical solution unless the isotherm is linear. However, in this case, an approximate description can be obtained using the pore diffusion model solutions but replacing D_e with an apparent diffusivity defined by [17]:

$$\tilde{D}_e = D_e + \frac{q_m}{C_0} \cdot D_s \quad (9)$$

4. Results and discussion

4.1. Uptake results

Batch uptake data for BSA on BRX-Q at different initial concentrations are shown in Fig. 2 in terms of solution concentration (C/C_0) and of the amount of protein adsorbed per unit particle volume ($\bar{q}$). The latter was calculated by material balance. From Fig. 2a, we see that all of the C/C_0 curves are nearly coincident for a substantial length of time (~100 s) during the initial stage of adsorption. At the lower

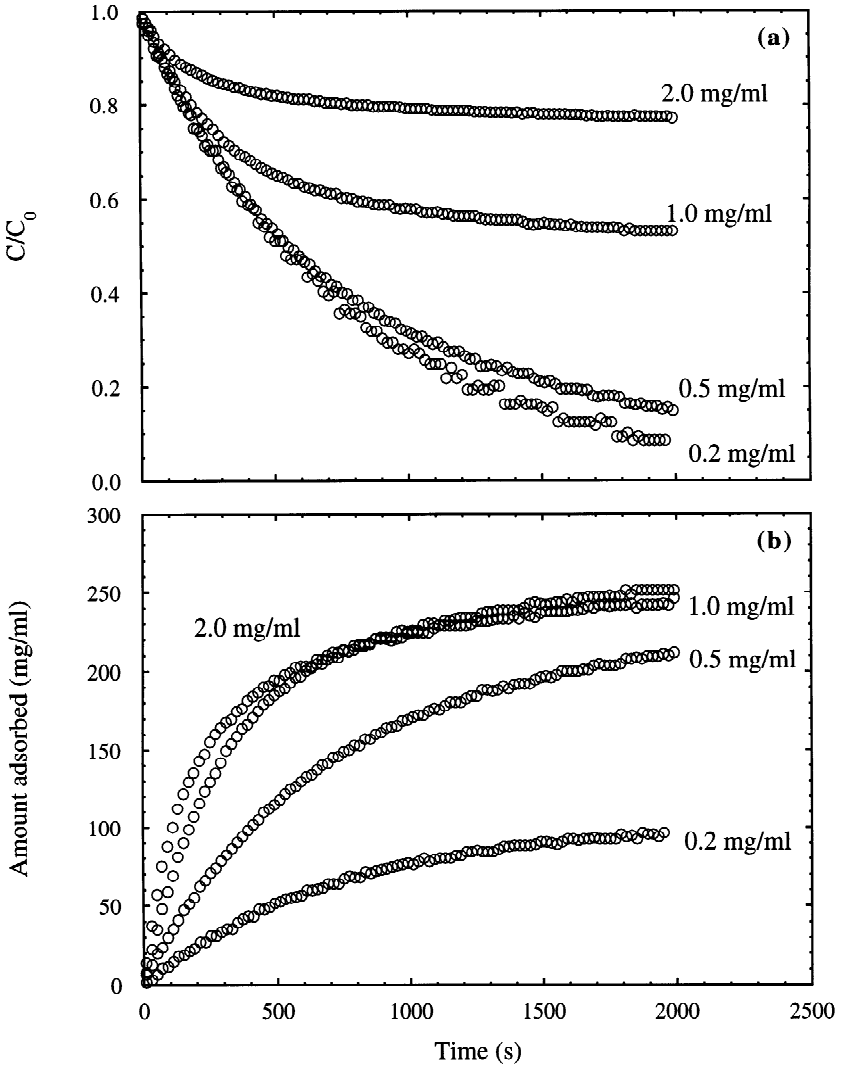

Fig. 2. Uptake curves for BSA on BRX-Q for different initial protein concentrations in agitated vessel: (a) normalized bulk fluid concentration and (b) amount adsorbed per unit particle volume.

initial concentrations, these curves remain nearly coincident for the entire duration of the experiment. This result indicates that the external resistance plays a substantial role. In fact, for film-resistance control with a highly favorable isotherm, from Eq. (2) we obtain the result [8,17]:

$$\frac{C}{C_0} = \exp\left(-\frac{3k_f}{r_p} \cdot t \right) \tag{10}$$

which is consistent with the data in Fig. 2a for short times and/or small concentrations. Considering the data as displayed in Fig. 2b, we see that mass transfer rates increase with protein concentration as C_0 is increased from 0.5 to 1 mg/ml, but do not increase very much when the concentration is doubled further to 2 mg/ml. For the experiment at $C_0 = 0.2$ mg/ml there is not enough protein to completely saturate the particle. Hence, $\bar{q}$ is small even for very long times.

Shallow-bed uptake results for BSA on BRX-Q showing the effects of protein concentration and of mobile phase velocity are given in Figs. 3 and 4, respectively. The effect of protein concentration is similar to that observed in batch experiments and the adsorption rates at 1 and 2 mg/ml are seen to be very similar. However, we can see that the same saturation capacity is approached even at 0.2 mg/ml, although at a substantially lower rate. The uptake curve is fairly linear for these conditions and this suggests again that the external resistance plays an important role at low concentrations. In this case, since the protein concentration remains constant, integration of Eq. (2) assuming film resistance control yields:

$$\bar{q} = \frac{3k_f}{r_p} \cdot C_0 t \tag{11}$$

which predicts a linear relationship between $\bar{q}$ and t. The results in Fig. 4 show that, for higher concentrations, the mobile phase velocity has no detectable effect on the uptake rate over the range 1200–2400 cm/h. This indicates that the media retains its structural integrity and that intraparticle convection does not play a significant role for these conditions.

Batch uptake data for BSA on BRX-QP are shown in Fig. 5. This material had been shown to have large, open pores with a very high size-exclusion limit for neutral macromolecules [1]. Adsorption of BSA is essentially irreversible on this media, but the capacity is lower than in BRX-Q [1]. In this case, compared to the data in Fig. 2a, the region where the C/C_0 curves (Fig. 5a) are superimposed is limited to extremely short times. Thus, external mass transfer does not play a significant role here. As seen in Fig.

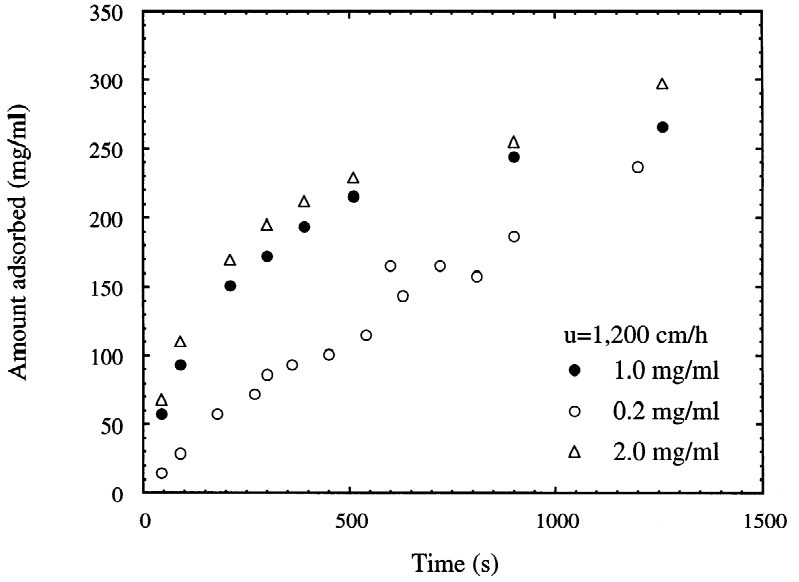

Fig. 3. Uptake curves for BSA on BRX-Q for different initial protein concentrations in shallow-bed apparatus at 1200 cm/h.

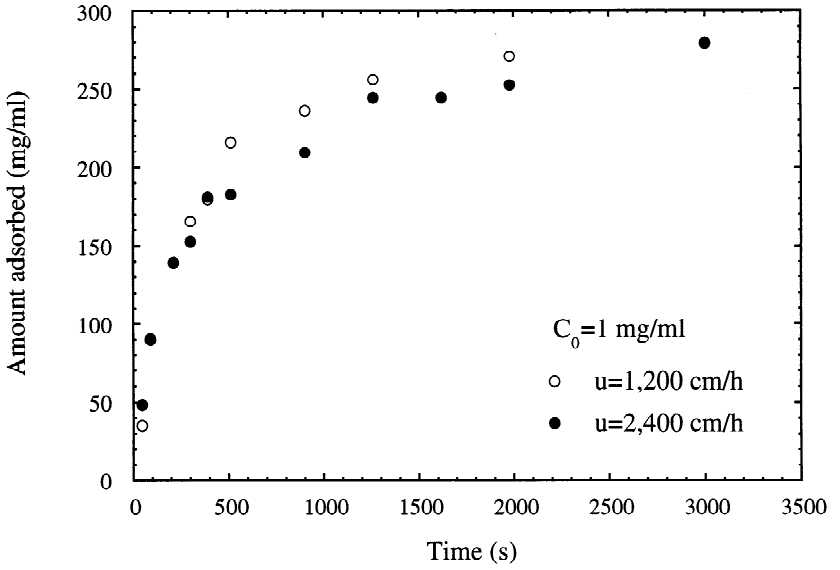

Fig. 4. Uptake curves for BSA on BRX-Q for different mobile phase velocities in shallow-bed apparatus at $C_0 = 1$ mg/ml.

5b, mass transfer rates are much lower than observed for BRX-Q and continue to increase as the protein concentration is raised from 1 to 2 mg/ml.

Finally, batch uptake curves for αCHY on BRX-S are shown in Fig. 6. The results are intermediate between those in Figs. 2 and 5. In particular, the time during which the C/C_0 curves coincide is appreciable, while the effect of protein concentration on the uptake rate is more pronounced in the 1–2 mg/ml range compared to BRX-Q.

4.2. Analysis of uptake curves

As evident from the preceding discussion, the relative importance of external and internal resistances and the intraparticle transport mechanism are different for the different materials studied. Thus, in order to obtain a consistent analysis of the data, we adopted an approach similar to that suggested by Yoshida et al. [5], where surface diffusion is neglected initially and the pore diffusivity is treated as a concentration-dependent adjustable parameter. Because the adsorption isotherms are very steep for these materials (see Ref. [1]), Eqs. (7) and (8) can be used with k_f and $\tilde{D}_e$ as adjustable parameters. In the case of BRX-Q and BRX-S, k_f could be determined precisely since the external resistance is clearly significant for short times and/or low concentrations. The resulting k_f values (Table 1) agree with previous determinations for proteins and correlations for mass transfer to small particles in agitated vessels [19,29]. For BRX-QP, however, because of the lower intraparticle mass transfer rates, the fit was insensitive to k_f. Thus, in this case we used the value obtained for the BRX-Q particles, which have a similar size. In any case, the error would be very small, since k_f plays only a minor role for BRX-QP.

Fig. 7 shows the fitted apparent diffusivity values $\tilde{D}_e$ normalized with respect to the free diffusivities reported by Tyn and Gusek [20] ($D_{BSA} = 6 \cdot 10^{-7}$ cm^2/s, $D_{\alpha CHY} = 9.3 \cdot 10^{-7}$ cm^2/s). As seen in this graph, the apparent diffusivity of BSA in BRX-Q far exceeds the free diffusivity and increases as the protein solution concentration is decreased. Shallow-bed and batch results agree when plotted versus C_0, indicating that intraparticle transport is independent of hydrodynamics for these conditions. Note that plotting the batch-determined $\tilde{D}_e$ values versus the initial concentration is reasonable since the fit tends to be biased toward early times. In contrast to the BRX-Q results, much lower apparent pore diffusivity values are obtained for BRX-QP. Here the ratio $\tilde{D}_e/D$ is much less than unity, as expected for diffusion through a tortuous pore network, and

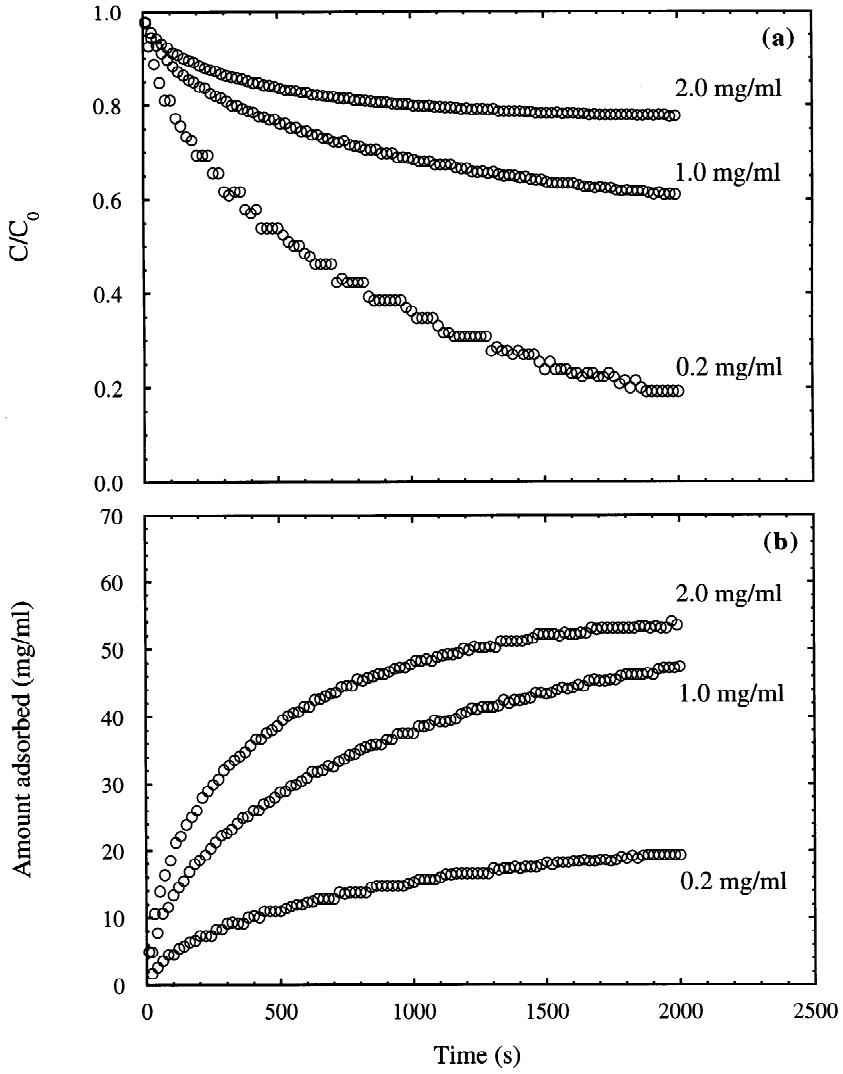

Fig. 5. Uptake curves for BSA on BRX-QP for different initial protein concentrations in agitated vessel: (a) normalized bulk fluid concentration and (b) amount adsorbed per unit particle volume.

essentially independent of solution concentration. For αCHY in BRX-S, the diffusivity ratio is less than unity. However, it increases significantly as the protein concentration is decreased.

We can now consider a physical interpretation of the apparent pore diffusivity data in light of the morphology of the three materials studied. BRX-Q was shown to have a very low size-exclusion limit for neutral macromolecules (e.g., $K_D \sim 0.02$ for Dextran T-40, which has an effective probe radius similar to BSA). Yet, this material exhibited an extremely high BSA binding capacity at low salt concentration ($q_m \sim 285$ mg/ml). Thus, for this material we can expect $D_e \sim 0$ and intraparticle transport to be dominated by D_s. Refitting the uptake curves using D_s as the sole adjustable parameter yields the calculated curves shown in Fig. 8. This was obtained from the numerical solution of Eqs. (1–2) obtained as discussed in Ref. [8]. In this case, a single, concentration-independent value of D_s (see Table 1) provides an excellent fit of all the uptake curves. Since partitioning of BSA in these particles is very

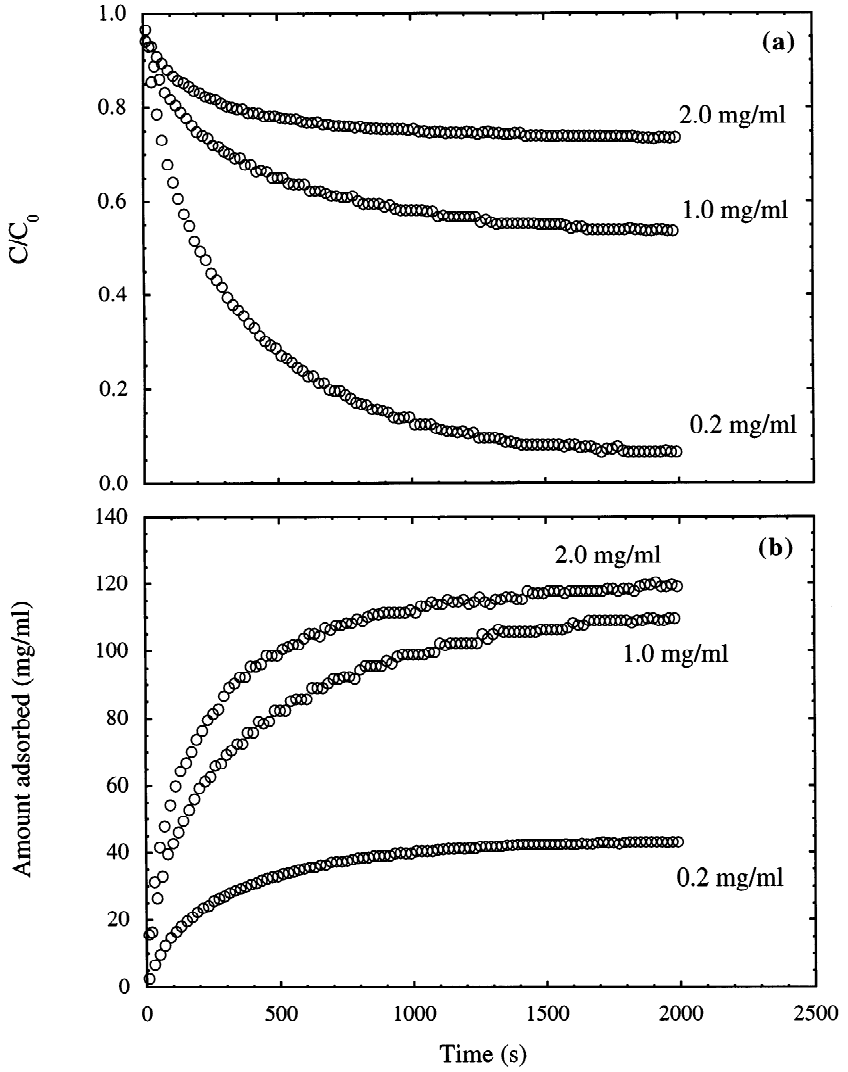

Fig. 6. Uptake curves for αCHY on BRX-S for different initial protein concentrations in agitated vessel: (a) normalized bulk fluid concentration and (b) amount adsorbed per unit particle volume.

Table 1
Mass transfer parameters

Material/protein	q_m [a] (mg/ml)	$\bar{d}_p$ [b] (μm)	k_f [c] (cm/s)	D_e (cm^2/s)	D_s (cm^2/s)
BRX-Q/BSA	285	89	$1.0\cdot10^{-3}$	–	$2.4\cdot10^{-9}$
BRX-QP/BSA	63	98	$1.0\cdot10^{-3}$	$6.2\cdot10^{-8}$	–
BRX-S/αCHY	125	63	$1.2\cdot10^{-3}$	$8.7\cdot10^{-8}$	$0.3\cdot10^{-9}$

[a] In pH 8.5, 50 m*M* Tris–HCl for BSA and in pH 6.5, 10 m*M* Na_2HPO_4 for αCHY [1].
[b] Mean particle diameter [1].
[c] In stirred-batch apparatus.

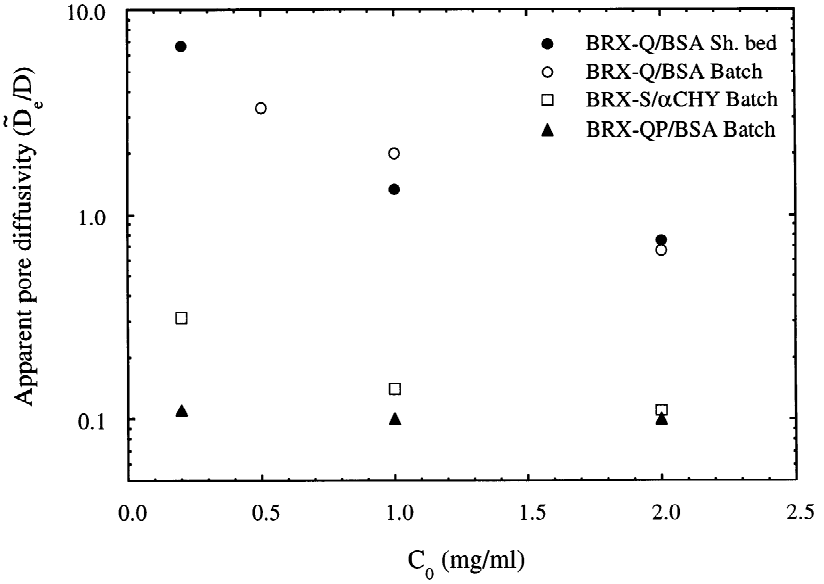

Fig. 7. Apparent pore diffusivity obtained at different protein concentrations in shallow-bed and stirred-batch contactors normalized with the free solution protein diffusivity.

favorable (i.e., $q_m/C_0 >> 1$), high intraparticle mass transfer rates can be obtained even if the true protein diffusivity in the gel is low. Moreover, since the isotherm is nearly rectangular [1], intraparticle mass transfer is essentially independent of protein solution concentration.

In the case of BRX-QP, the media contains large open pores with a very high size-exclusion limit.

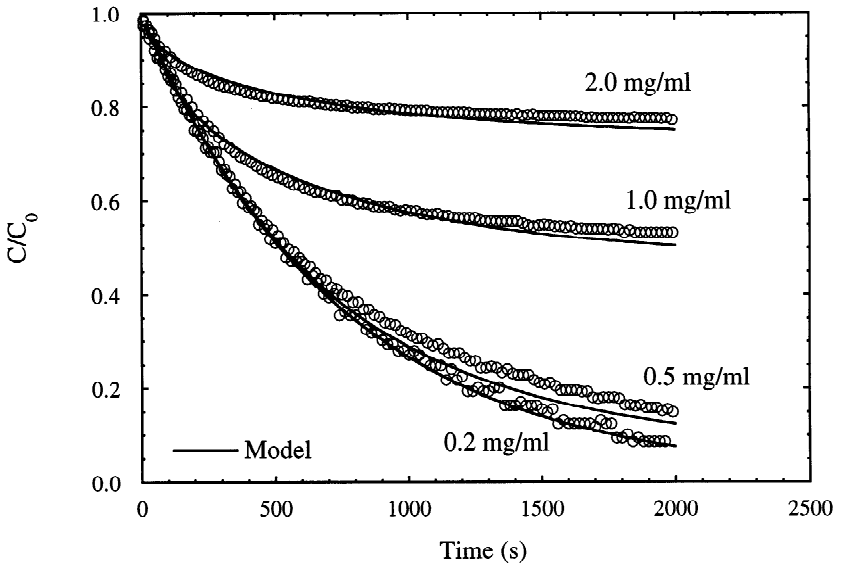

Fig. 8. Fit of BRX-Q/BSA batch uptake curves with homogeneous diffusion model ($D_e = 0$, $D_s = 2.4 \cdot 10^{-9}$ cm^2/s, $k_f = 0.001$ cm/s).

Moreover, the adsorption isotherm is irreversible [1]. Thus, surface diffusion is negligible and a constant value of $D_e = 6.2 \pm 0.2 \cdot 10^{-8}$ cm^2/s provides a good fit of the data over the entire range. For BRX-S, however, pore and surface diffusion are similar in magnitude at protein concentrations around 1 mg/ml. A fit of the data in Fig. 7 for these particles with Eq. (9) gives the values of D_e and D_s reported in Table 1.

4.3. Column behavior

Representative breakthrough curves for BSA on BRX-Q and BRX-QP columns, and for αCHY on a BRX-S column are shown in Figs. 9–11 with C/C_F plotted as a function of protein loading per unit column volume ($=uC_Ft/L$). The dynamic bed capacity (DBC) is given by the x-axis for a chosen C/C_F value. In all three cases, the DBC decreases

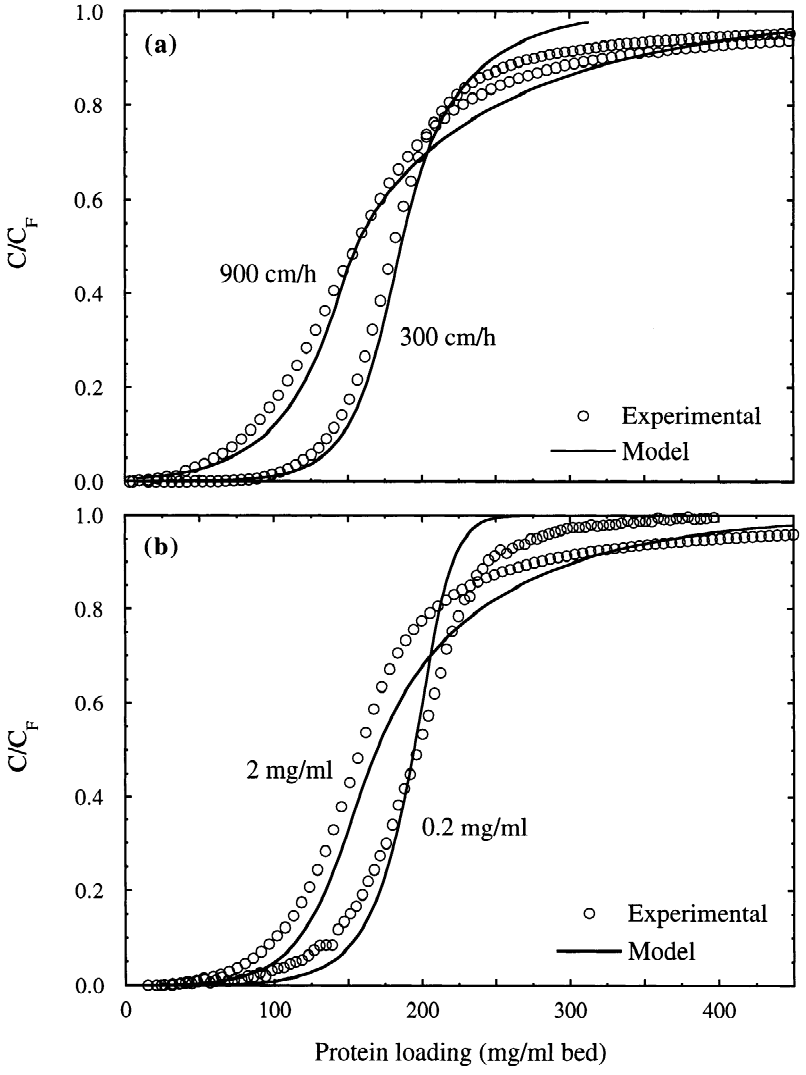

Fig. 9. Breakthrough curves for BSA on BRX-Q column: (a) effect of mobile phase velocity ($L = 1.6$ cm) at 1 mg/ml feed concentration and (b) effect of feed concentration at $u = 300$ cm/h ($L = 1.5$ cm). Lines are predictions based on homogeneous diffusion model with $D_s = 2.4 \cdot 10^{-9}$ cm^2/s.

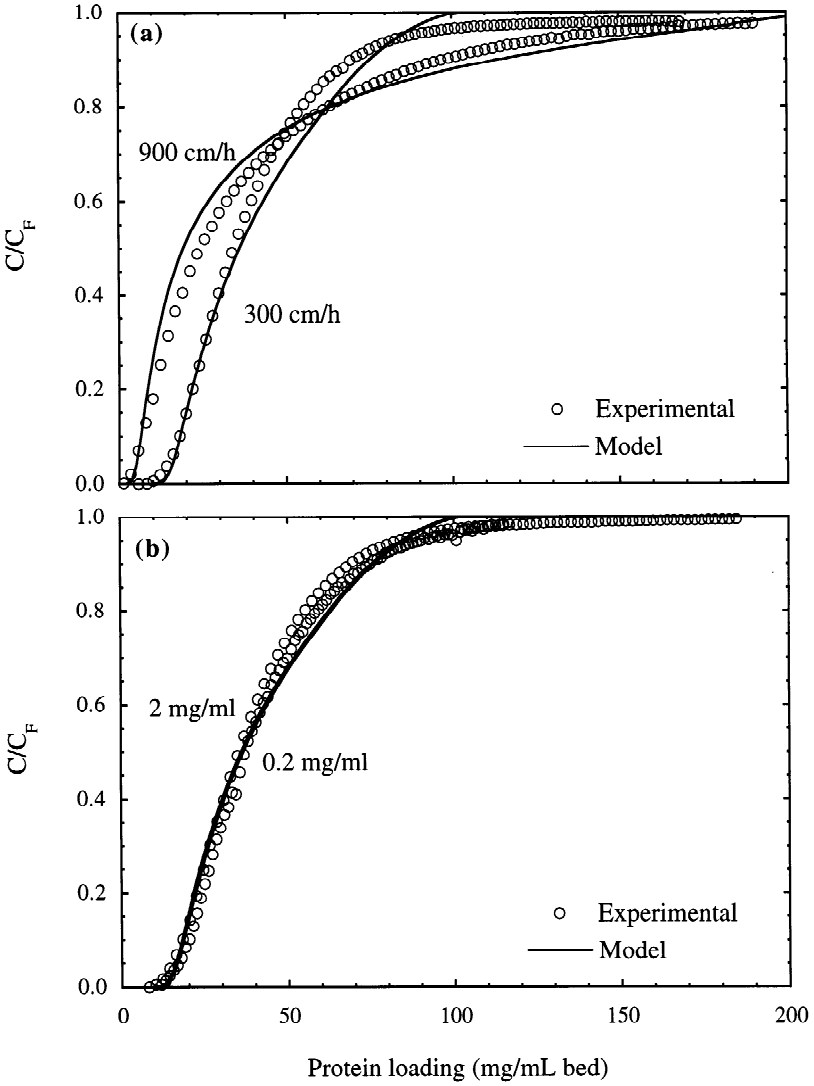

Fig. 10. Breakthrough curves for BSA on BRX-QP column: (a) effect of mobile phase velocity ($L=5.4$ cm) at 1 mg/ml feed concentration and (b) effect of feed concentration at $u=300$ cm/h ($L=5.4$ cm). Lines are predictions based on pore diffusion model with $D_e=6.2\cdot10^{-8}$ cm^2/s.

with increasing mobile phase velocity. However, the effect of feed concentration is different for the different media. In the case of BRX-Q, the DBC increases as the protein concentration is reduced from 2 to 0.2 mg/ml. Conversely, the breakthrough curve for BRX-QP is essentially independent of feed concentration when plotted in this form. The runs at 1 mg/ml exhibited consistent trends. The origin of this behavior is to be found in the different mass transfer mechanisms. In the case of BRX-Q, intraparticle mass transfer is dominated by surface or gel-diffusion and is independent of solution concentration. Thus, as the concentration is decreased, the apparent pore-diffusivity becomes larger leading to a sharper breakthrough curve. This effect is somewhat mitigated by the external mass transfer resistance, however, which if acting alone would give the opposite effect. For BSA on BRX-QP,

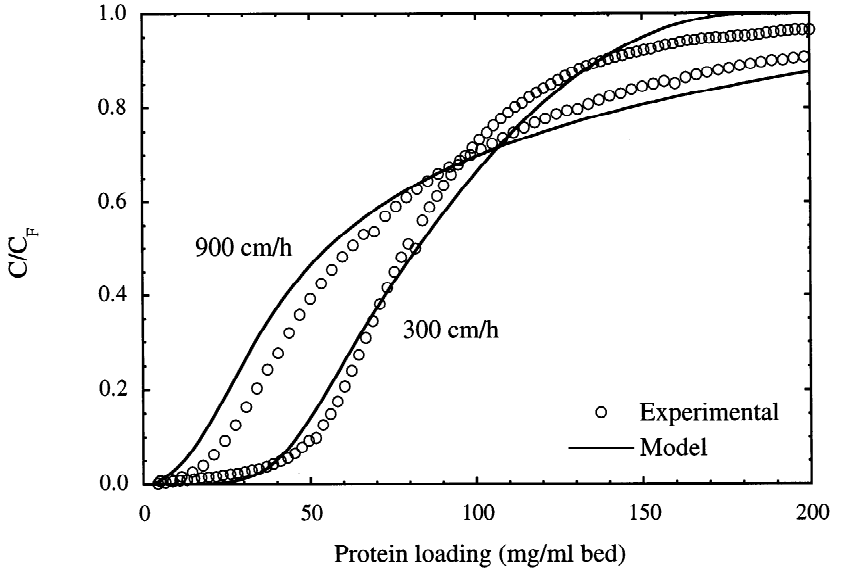

Fig. 11. Breakthrough curves for 1 mg/ml αCHY on BRX-S column at different mobile phase velocities ($L=1.6$ cm). Lines are predictions based on pore diffusion model with $\bar{D}_e = 13\cdot 10^{-8}$ cm^2/s.

intraparticle transport is dominated by diffusion through an open pore network. Hence, intraparticle mass transfer varies in direct proportion to solution concentration. However, since the number of transfer units, $N_{\text{pore}} = 15\cdot(1-\epsilon_b)\cdot D_e L/ur_p^2$, which is independent of C_F determines the steepness of the breakthrough curve [17], the DBC does not vary with C_F.

Figs. 9–11 also show model predictions for each material. We assumed negligible axial dispersion and used the rate parameters summarized in Table 1, except for k_f that was estimated using the Carberry correlation [8,17]:

$$k_f = 1.15\cdot\frac{u}{\epsilon_b}\cdot\left(\frac{u\bar{d}_p}{\nu}\right)^{-1/2}\cdot\left(\frac{\nu}{D}\right)^{-2/3} \tag{12}$$

In the case of BRX-Q, we solved Eqs. (1) and (3) numerically, together with a Langmuir isotherm fit of the equilibrium data given in Ref. [1]. The numerical solution was obtained using orthogonal collocation with a method similar to that of Saunders et al. [30]. For BSA on BRX-QP, since pore diffusion is dominant and the isotherm is irreversible, the analytical solution of Eqs. (1) and (3) assuming a rectangular isotherm was used. Under constant pattern conditions, the latter is given by [27]:

$$(\tau_1 - 1)\cdot N_{\text{pore}} = \frac{15}{\sqrt{3}}\cdot\tan^{-1}\left[\frac{2\eta+1}{\sqrt{3}}\right] - \frac{15}{2}\cdot\left[\ln(1+\eta+\eta^2) - \frac{1}{3}\right] + \frac{5}{\text{Bi}}\cdot\left[\ln(1-\eta^3)+1\right] - \frac{5\pi}{2\sqrt{3}} \tag{13}$$

where:

$$\tau_1 = \frac{\left(\frac{ut}{L} - \epsilon_b\right)}{\Lambda} \tag{13a}$$

$$N_{\text{pore}} = \frac{15\cdot(1-\epsilon_b)\cdot D_e L}{ur_p^2} \tag{13b}$$

$$\eta = \left(1 - \frac{C}{C_F}\right)^{\frac{1}{3}} \tag{13c}$$

$$\Lambda = \frac{(1-\epsilon_b)\cdot q_m}{C_F} \tag{13d}$$

This form requires $N_{\tau_1} > 2.5 + 1/\text{Bi}$, which was satisfied only approximately for the BRX-QP data at 300 cm/h. Thus, the general solution of Weber and Chakravorti [27] was used instead for an accurate prediction at all flow-rates. As seen in Fig. 10, the

agreement between predicted and experimental breakthrough curves is excellent, especially in the early portion of the curves that determines the useful DBC. As observed experimentally, the predicted profile is independent of feed concentration when plotted versus the amount of protein fed to the column. In the case of BRX-S, in principle one needs to account for parallel pore and surface diffusion, but this would require a complex numerical solution. However, as seen in Fig. 11, we can obtain a reasonable prediction with Eq. (13) using $\tilde{D}_e$ in lieu of D_e. The former was calculated from Eq. (9).

Finally, we can see that in all three cases, the breakthrough curves exhibit a final tailing portion that is not predicted exactly by any of the models. There is greater tailing for BRX-Q, and this affects the agreement between the entire experimental and predicted curves (e.g., Fig. 9). A tailing behavior is often seen with proteins, and especially BSA (cf. Refs. [31–33]). A few authors [34,35] have advanced an explanation of tailing breakthrough curves observed for proteins in terms of steric-hindrance effects (the so-called ''parking problem''). Another possibility is that tailing was caused by hydrodynamic effects such as axial dispersion [36], flow non-uniformity, or extracolumn contributions that are sometimes significant in short columns [37]. To test this possibility we explored the effect of column length on the breakthrough behavior of BSA with BRX-Q, which exhibits the highest transport rates. Experimental results and model predictions comparing breakthrough curves obtained in columns with packed bed heights of 1.6 and 3.3 cm are shown in Fig. 12. The tailing behavior is clearly very similar in the two columns and so is the agreement between experimental data and predictions, suggesting that flow non-idealities played a negligible role in these experiments. In fact, even for the short column, because of the high capacity of the stationary phase a constant pattern behavior is achieved. A final possibility to explain the tailing behavior is that it was caused by impurities present in the BSA sample. Indeed, SEC analyses of the BSA used in this work using a 30×1 cm Superdex 200 column (Pharmacia) showed that a significant amount of BSA dimer, approximately 5%, was present. The dimer is apparently more strongly held than the monomer. Thus, its effect was manifested primarily in the tailing portion of the breakthrough curve. In fact, no dimer was detectable by SEC in fractions collected from the column effluent during breakthrough. At the same time, the effect of the dimer on the batch experiments used to determine transport coefficients was likely small since no chromatographic separation

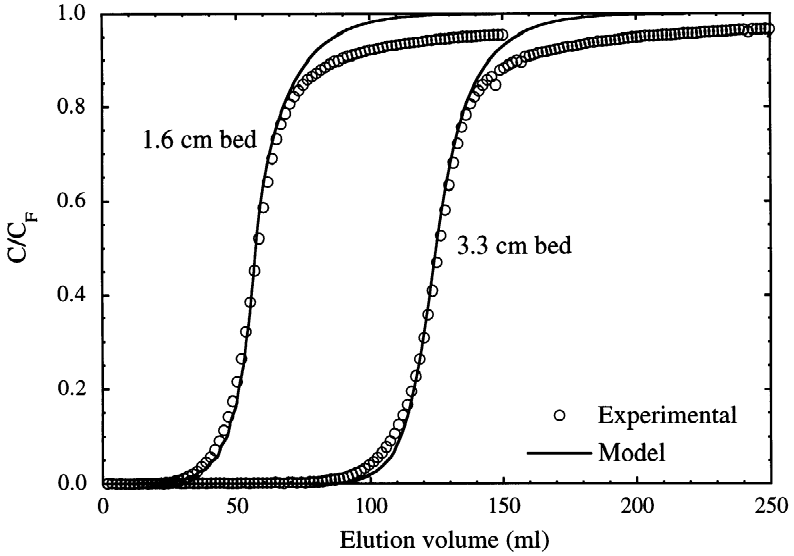

Fig. 12. Breakthrough curves for 1 mg/ml BSA on BRX-Q column: effect of column length at $u=300$ cm/h. Lines are predictions based on homogeneous diffusion model with $D_s=2.4\cdot10^{-9}$ cm^2/s.

occurred for those conditions. In any case, however, the model accurately predicts the initial portion of the breakthrough curve, which is most important from a practical viewpoint.

5. Conclusions

We have systematically investigated mass transfer in novel stationary phases for ion-exchange of proteins based on hydrophilic acrylamido and vinyl monomers having different morphologies. These materials have a heterogeneous structure and sufficient rigidity for column operation at reasonably high flow-rates of the mobile phase. Different mechanisms were found to be dominant in the three materials. The paradoxical conclusion that the particles having the smallest size-exclusion limit for neutral probes have the highest static capacity *and* the highest mass transfer rates is amply supported by the experimental results. In terms of a conceptual model, this implies a dominance of diffusion through gel-pores where the protein continuously interacts with the ion-exchange sites. Much lower rates (and capacity) are obtained with a material synthesized to have a network of large, open pores and where pore diffusion is dominant. Intermediate rates are observed for a material where parallel diffusion paths exist.

Finally, we can address the issue of intraparticle convection. Shallow-bed experiments have shown that the mobile phase velocity does not have a significant effect on intraparticle mass transfer rates in BRX-Q. Moreover, the column behavior is consistent with rates observed in an agitated vessel. Are there any conditions, then, where intraparticle convection is likely to have an effect? The case of αCHY in BRX-S can be used as an illustration. The particles have a macroporosity of about 0.42 and mean particle size of 63 μm [1]. Although the mean pore diameter could not be calculated exactly, it is evident from TEM images [1] that this is in the range 0.2–0.4 μm. In this case, assuming $\epsilon_b = 0.35$, Eq. (6) gives $F = 2\text{–}8 \cdot 10^{-4}$. Correspondingly, using the experimental value of $D_e = 8.7 \cdot 10^{-8}$ cm^2/s, we have $Pe_{intra}/u = 2.4\text{–}9.5$. In turn, since values of $Pe_{intra} > 10$ are required to see any enhancement of intraparticle mass transfer, we can conclude that mobile phase velocities in the range 3800–15 000 cm/h would be needed to see a positive impact. Based on these estimates, intraparticle convection could lead to a doubling of uptake transfer rates only if we operated these particles at velocities greater than 11 000 cm/h. The results are, of course, quite different with the BRX-Q particles. In this case, no enhancement by intraparticle convection is possible. Yet, higher mass transfer rates of BSA are observed as a result of surface diffusion and the very favorable partitioning of the protein in this medium. A final consideration regards the possible effect of salt concentration on the intraparticle mass transfer rates and mechanisms. While pore diffusivities are expected to be nearly independent of salt concentration, adsorbed phase diffusivities could be significantly affected. This effect was not considered in this work and will be the subject of a future communication.

6. Nomenclature

Bi	Biot number defined by Eq. (7f)
c	Protein concentration in pore fluid, mg/ml
C	Protein concentration in solution, mg/ml
C_F	Feed protein concentration, mg/ml
C_0	Initial protein concentration in solution, mg/ml
$\bar{d}_p$	Average particle size, cm
D	Free solution diffusivity, cm^2/s
D_e	Pore diffusivity, cm^2/s
D_s	Adsorbed-phase diffusivity in homogeneous diffusion model, cm^2/s
D_L	Axial dispersion coefficient, cm^2/s
$D_{e,conv}$	Convection augmented effective diffusivity, cm^2/s
$\tilde{D}_e$	Apparent effective diffusivity defined by Eq. (9), cm^2/s
F	Intraparticle velocity fraction, Eq. (6)
k_f	External film mass transfer coefficient, cm/s
K_D	Distribution coefficient
L	Bed length, cm
N_{pore}	Number of transfer units for pore diffusion control
Pe_{intra}	Peclet number for intraparticle convection and diffusion ($=Fur_p/3D_e$)
q	Protein concentration in particle, mg/ml

q_m	Adsorption capacity, mg/ml
$\bar{q}$	Average concentration in particle, mg/ml
r_p	Particle radius, cm
r_{pore}	Pore radius, nm
t	Time, s
u	Mobile phase superficial velocity, cm/s
z	Bed length coordinate, cm

Greek symbols

ϵ_b	Extraparticle void fraction
ϵ_p	Particle porosity
ν	Kinematic viscosity, cm^2/s

Acknowledgements

This research was supported by Bio-Rad Laboratories, Inc., and by NSF Grant No. CTS-9709670.

References

[1] A.K. Hunter, G. Carta, J. Chromatogr. A 897 (2000) 65.
[2] B.H. Arve, A.I. Liapis, AIChE J. 33 (1987) 179.
[3] G.L. Skidmore, B.J. Horstmann, H.A. Chase, J. Chromatogr. 498 (1990) 113.
[4] M.M. Hossain, D.D. Do, Chem. Eng. J. 49 (1992) B29.
[5] H. Yoshida, M. Yoshikawa, T. Kataoka, AIChE J. 40 (1994) 2034.
[6] A. Tonga, A.I. Liapis, D.J. Siehr, J. Chromatogr. A 686 (1994) 21.
[7] K. Miyabe, G. Guiochon, Biotechnol. Prog. 15 (1999) 740.
[8] L.E. Weaver Jr., G. Carta, Biotechnol. Prog. 12 (1996) 342.
[9] C. Chang, A.M. Lenhoff, J. Chromatogr. A 827 (1998) 281.
[10] J.J. Meyers, A.I. Liapis, J. Chromatogr. A 827 (1998) 197.
[11] H. Tsou, E.E. Graham, AIChE J. 31 (1985) 1959.
[12] G.F. Bloomingburg, G. Carta, Chem. Eng. J. 55 (1994) B19.
[13] R.K. Lewus, G. Carta, J. Chromatogr. A 865 (1999) 155.
[14] P.G. Righetti, T. Caravaggio, J. Chromatogr. 127 (1976) 1.
[15] R.K. Lewus, F.H. Altan, G. Carta, Ind. Eng. Chem. Res. 37 (1998) 1079.
[16] G. Guiochon, S. Golshan-Shirazi, A. Katti, Fundamentals of Preparative and Nonlinear Chromatography, Academic Press, Boston, MA, 1994.
[17] M.D. LeVan, G. Carta, C.M. Yon, in: D.W. Green (Ed.), Perry's Chemical Engineers Handbook, 7th ed., McGraw-Hill, New York, 1997, Section 16.
[18] W.M. Deen, AIChE J. 33 (1987) 1409.
[19] M.A. Fernandez, G. Carta, J. Chromatogr. A 746 (1996) 169.
[20] M.T. Tyn, T.W. Gusek, Biotechnol. Bioeng. 35 (1990) 327.
[21] A.E. Rodrigues, Z. Lu, J.M. Loureiro, Chem. Eng. Sci. 46 (1991) 2765.
[22] G. Carta, M.E. Gregory, D.J. Kirwan, H.A. Massaldi, Sep. Technol. 2 (1992) 62.
[23] A.I. Liapis, M.A. McCoy, J. Chromatogr. 599 (1992) 87.
[24] D.D. Frey, E. Schweinheim, Horváth, Biotechnol. Prog. 9 (1993) 273.
[25] G. Carta, Chem. Eng. Sci. 50 (1995) 887.
[26] G. Carta, A.E. Rodrigues, Chem. Eng. Sci. 48 (1993) 3927.
[27] T.W. Weber, R.K. Chakravorti, AIChE J. 20 (1974) 228.
[28] H. Yoshida, T. Kataoka, D.M. Ruthven, Chem. Eng. Sci. 39 (1984) 1489.
[29] C.L. Borst, D.S. Grzegorczyk, S.J. Strand, G. Carta, React. Polym. 32 (1997) 25.
[30] M.S. Saunders, J.B. Vierow, G. Carta, AIChE J. 35 (1989) 53.
[31] A.E. Rodrigues, J.M. Loureiro, C. Chenou, M. Reundeles de la Vega, J. Chromatogr. B 664 (1995) 233.
[32] E. Hansen, J. Mollerup, J. Chromatogr. A 827 (1998) 259.
[33] G. Iberer, R. Hahn, A. Jungbauer, LC·GC 17 (1999) 999.
[34] X. Jin, J. Talbot, N.-H.L. Wang, AIChE J. 40 (1994) 1685.
[35] G. Garke, R. Hartmann, N. Papamichael, W.-D. Deckwer, F.B. Anspach, Sep. Sci. Technol. 34 (1999) 2521.
[36] A. Acrivos, Chem. Eng. Sci. 13 (1960) 1.
[37] O. Kaltenbrunner, A. Jungbauer, S. Yamamoto, J. Chromatogr. A 760 (1997) 41.